Title	Mechanical properties and reciprocating sliding tribological behaviors of γ-tial substrate and plasma-based mo–si–ti coating
Author(s)	Fengkun Li, Rajdeep Singh Rawat, Pingze Zhang, Dongbo Wei, Ka Yang and Bo Dang

The final publication is available at: https://doi.org/10.1016/j.jmrt.2023.07.261

Mechanical properties and reciprocating sliding tribological behaviors of γ-TiAl substrate and plasma-based Mo-Si-Ti coating

Fengkun Li[a,b,c], Rajdeep Singh Rawat[b], Pingze Zhang[a,c], Dongbo Wei[a,c], Ka Yang[a,c], Bo Dang[a,c]

a College of Materials Science and Technology, Nanjing University of Aeronautics and Astronautics, Nanjing, Jiangsu, 211106, China
b Natural Sciences and Science Education, National Institute of Education, Nanyang Technological University, Singapore 637616, Singapore
c Key Laboratory of Materials Preparation and Protection for Harsh Environment (Nanjing University of Aeronautics and Astronautics), Ministry of Industry and Information Technology, Nanjing, Jiangsu, 211106, China.

Abstract

Plasma Mo-Si-Ti coating including the $(Ti, Mo)_5Si_3$, $MoSi_2$ and TiSi was prepared on γ-TiAl surface to improve the wear resistance. The coating had 12-μm deposition layer and 5-μm diffusion layer, as well as gradual decrease of grain size from substrate to coating, providing gradient structure and high fracture toughness. Hardness (H), elasticity modulus (E), H/E and H^3/E^2 values of substrate and coating were 8.4 and 19.6 GPa, 167.2 and 251.8 GPa, 0.050 and 0.078, and 0.021 and 0.119 GPa, indicating that coating had high hardness, resistance to plastic deformation and load bearing capacity. During friction, both the substrate and coating showed abrasive and oxidative wear. The substrate flaked off in the form of large wear debris, causing the high wear rate. However, oxide film and compacted layer of fine debris made the wear rates of substrate to decrease as the load increased. The coating released most of external stress in the form of elastic work, showing high load-bearing capacity. High fracture toughness inhibited the generation of cracks and reduced the spallation of coating. Moreover, fine grains promoted the generation of oxide film on coating surface and improved the adhesion between oxide film and coating. Meanwhile, the presence of oxide film resulted in a reduction of wear rate as the load increased. The excellent nanomechanical properties and fracture toughness reduced the fracture of coating and reduced the specific wear rate of γ-TiAl by about 98%, which could effectively improve the wear resistance of γ-TiAl at room temperature.

Keywords: γ-TiAl; Mo-Si-Ti gradient coating; nanoindentation; wear mechanism.

1. Introduction

γ-TiAl is regarded as the most promising material for the low pressure turbine (LPT) blades due to the high elastic modulus (160-180 GPa), specific strength above 600 ℃ and low density (3~4 g/cm^3) [1–3]. However, the formation of non-dense oxide film causes the γ-TiAl to suffer severe oxidation during service [4,5]. Besides its poor oxidation resistance, the limited wear resistance due to low hardness (320 HV) is a crucial problem that restricts the application of γ-TiAl. For example, wear occurs between the blades and the engine disc due to centrifugal force and vibration [6–8].

As a refractory metal silicide, Mo_5Si_3 exhibits good properties such as high melting point, hardness and modulus of elasticity and is considered to be a high temperature structural material with great potential. However, the generation and volatilization of MoO_3 or MoO_2 makes it difficult to form dense oxide film in the environment of 400-1000 ℃ (“pesting” phenomenon), limiting the application of Mo_5Si_3. The addition of Ti in the Mo-Si system can form $(Ti,Mo)_5Si_3$, which reduce the formation of MoO_3 or MoO_2 because of the low mobility of Mo as well as the low driving force for the MoO_3 and MoO_2, and thus inhibits the “pesting” phenomenon [9–12]. As a result, Mo-Si-Ti alloy with the $(Ti,Mo)_5Si_3$ phase exhibit excellent oxidation resistance at high temperature [13–18]. Meanwhile, the wear and oxidation usually occur on the material surface. Therefore, the excellent mechanical properties as well as the oxidation resistance make the Mo-Si-Ti coating suitable for application as a protective layer on γ-TiAl surface.

However, as a wear resistant coating, it is important to note that the obvious difference in the elastic modulus between the γ-TiAl and Mo-Si-Ti coating causes an uncoordinated deformation at the interface between the substrate and coating. After losing the support of γ-TiAl, the coating will easily fracture under the unbalanced stress field and lose its protective effect, which is a key problem for the Mo-Si-Ti coating. To solve this problem, a Mo-Si-Ti coating with a gradient structure was prepared in this study, which could avoid the sudden changes of mechanical properties between the substrate and the coating, reducing the fracture of coating. As a surface modification technology, double glow plasma alloying technology (DGP) provides a suitable method

for the preparation of the Mo-Si-Ti coating [19–23]. The Mo-Si-Ti coating with diffusion layer could be obtained based on the thermodynamically favorable reaction and ion bombardment, achieving the continuous change of composition as well as the structure between the coating and substrate. The gradient structure can increase the fracture toughness and crack resistance of the Mo-Si-Ti coating by acting as a buffer zone between the coating and the substrate. When the cracks come into contact with the ductile substrate, tensile stress causes local deformation in the ductile phase, consuming energy during crack propagation [24]. Alternatively, the crack tends to deflect and expand along the interface when it extends into a phase interface with a strong strain field, generating a crack bridge and allowing some of the work to dissipate [25].

The aim of this paper was to prepare Mo-Si-Ti coating with gradient structure on the γ-TiAl surface and studied the mechanical properties of Mo-Si-Ti coating based on the structural characteristics, nanomechanical properties and fracture toughness. The correlation between microstructure, mechanical properties and tribological behavior were further analyzed.

2. Materials and experimental procedure

2.1 Coating preparation

The γ-TiAl (provided by Central Iron & Steel Research Institute, Beijing, CN) with the composition of 46.5 wt.% Al, ≤1.5 wt.% V, ≤ 1 wt.% Cr, ≤ 0.20 wt.% Nb, ≤ 0.10 wt.% C, and the balance of about 50 wt% of Ti was selected as substrate material. The γ-TiAl was cut into 15×15×5 mm^3 squares by wire cutting (DK7735 electrical-discharge wire-cutting machine; Suzhou Shengma Numerical Control Technology Co., Ltd., Suzhou, CN), after which the surface was polished to a roughness of less than 0.2 μm by sandpaper and then the sample was cleaned with alcohol (QREC; QREC (ASIA) SDN BHD, Rawang, MYS) and acetone (QREC; QREC (ASIA) SDN BHD, Rawang, MYS). The Mo-Si-Ti target (provided by Zhongnuo Advanced Material (Beijing) Technology Co., Ltd., Beijing, CN) with dimensions of 100 mm diameter and 5 mm thickness were made by a powder metallurgy process, and consisted of 10 at.% Mo, 35 at.% Si, and 55 at.% Ti. The Mo, Si and Ti powders were ball-milled with tungsten carbide balls for 1 h, and then pressed and sintered in a mold at 750 ℃, 950 ℃, and

1700 ℃ for 45 min, 45 min, and 2 h, respectively. Finally, the target was removed from the mold after the temperature was cooled down to room temperature, and then polished and cleaned. γ-TiAl and target were placed in a vacuum chamber of DGP device (The equipment was developed by our research group and made by Anhui Jiashuo Vacuum Technology Co., Ltd., Anhui, CN) during coating preparation process. The distance between the γ-TiAl and target was 15 cm. Argon was used as the working gas to maintain the DGP chamber pressure at 38 Pa. Then, 450 V and 850 V cathode voltages were applied to substrate and target, respectively. Argon was ionized into argon ions, and continuously moved toward the target and sputtered out target elements, which were then deposited on the γ-TiAl surface. The deposition process was maintained for 3 h. A comprehensive description of the DGP technology could be accessed in the existing literature [21, 22].

2.2 Characterization

The surface and cross-sectional morphology and EDS (energy dispersive spectroscopy) line scanning were analyzed by scanning electron microscope (SEM) (HITACHI S-4800; Hitachi High-Tech Co., Ltd., Tokyo, JPN) equipped with an EDS detector. X-ray Diffraction (XRD) (Bruker-D8 ADVANCE; Bruker Corporation, Massachusetts, US) analysis was employed to determine the phase composition. The X-ray Diffraction test employed a Cu Kα radiation source operating at 40 kV and 40 mA with a scanning angle (2θ) range of 20-90° and the step size of 0.02°.

The nanomechanical properties of γ-TiAl substrate and coating were measured by Nanoindentation (Nanotest Vantage; Micro Materials Co., Ltd., Wrexham, UK). All samples were tested using maximum load of 50 mN, loading rates of 5 mN/s, and holding time of 10 s. To ensure the reliability of the experimental data, five groups of parallel tests were performed. The γ-TiAl substrate and coating were indented using a Vickers indenter (HXS-100AY; Nanjing Santak Instrument Co., Ltd., Nanjing, CN) at load of 300 g with holding time of 15 s. Cracks around the indent imprints were then observed by scanning electron microscopy (HITACHI S-4800; Hitachi High-Tech Co., Ltd., Tokyo, JPN) to study their toughness.

The tribological behaviors of γ-TiAl substrate and coating at room temperature

was tested using the CFT-I friction and wear testing machine (CFT-I; Zhongkeyuan Institute of Chemical Physics, Lanzhou, CN) at different loads of 420, 620, 820 g and a constant sliding speed of 400 r/min. Whole sliding length was 5 mm. Si_3N_4 ball with a diameter of 5 mm (provided by KOVE bearing Co., Ltd., Zhejiang, CN) was employed as the friction ball. The morphology of wear track, debris and friction ball were observed by scanning electron microscopy (HITACHI S-4800; Hitachi High-Tech Co., Ltd., Tokyo, JPN). The three-dimensional (3D) morphologies of wear tracks were test by three-dimensional optical profilometer (CONTOUR GT-K; Bruker Corporation, Massachusetts, US). The wear volume of the wear track was obtained by analyzing the 3D profile with software (RtecInsight; Rudolph Technologies, Inc., California, US). The specific wear rate, K, could be calculated using Eq. (1).

$$K = \frac{V}{PS} \tag{1}$$

where V represents the wear volume (mm^3), S represents the whole sliding distance (m) and P represents the load (N).

3. Results and discussion

3.1. Microstructure analysis of as-deposited Mo-Si-Ti coating

Fig. 1 depicted the morphology including surface and cross-sectional, EDS line scanning, transmission electron microscope dark-field (TEM-DF) image and X-ray diffraction pattern of Mo-Si-Ti coating, which showed a typical coating characteristic prepared by DGP technology i.e., pits caused by argon ion bombardment (Fig. 1a) as well as diffusion layer (Fig. 1b). The cross-sectional morphology showed that the coating was consisted of a 5 μm diffusion layer and a 12 μm deposition layer. The argon ions bombarded the γ-TiAl surface continuously and created the defects, such as the vacancies, grain boundaries and others, which promoted the formation of a 5 μm diffusion layer as buffer between the substrate and the coating. Mo, Si and Ti from the coating diffused into the substrate while Ti and Al from the substrate diffused into the coating under the thermodynamically favorable reaction. In addition to the compositional gradient, the coating exhibited a structure gradient. As shown in TEM-DF image of the substrate-coating cross-section in Fig. 1(c), the cross section consisted

of three parts. The first part was the area away from the substrate surface (Area Ⅰ) having a grain size of about 1 μm. The second part (Area Ⅱ) was the area at a distance of 0-0.3 μm under the substrate surface where the substrate grain refinement layer appeared and the grain size was about 0.1-0.2 μm. The continuous bombardment of argon ions and the stresses generated by the ion bombardment will result in the fragmentation of the grains on the surface of the substrate and lead to a decrease of the grain size [26]. Meanwhile, the increase of grain boundaries caused by grain refinement also promoted the interdiffusion of Al, Ti, Mo and Si. The third part (Area Ⅲ) was the coating with smaller grain size of 20 – 50 nm. The grain size decreased from the γ-TiAl to the coating, which promoted the gradient structure. According to the XRD result shown in Fig. 1d, the coating was primarily consisted of the $(Ti, Mo)_5Si_3$ phase, with some phases of $MoSi_2$ and TiSi. The diffraction peak of the $(Ti, Mo)_5Si_3$ phase was shifted to a higher angle compared to the peak of the Ti_5Si_3 phase (PDF 01-078-1429) as Mo replaced some Ti. According to Bragg diffraction equation, Mo with a smaller atomic radius (0.139 nm) replaced Ti with a larger atomic radius (0.146 nm), leading to a decrease in lattice spacing. As a result, the diffraction peak angle increased and caused a shift towards higher angle.

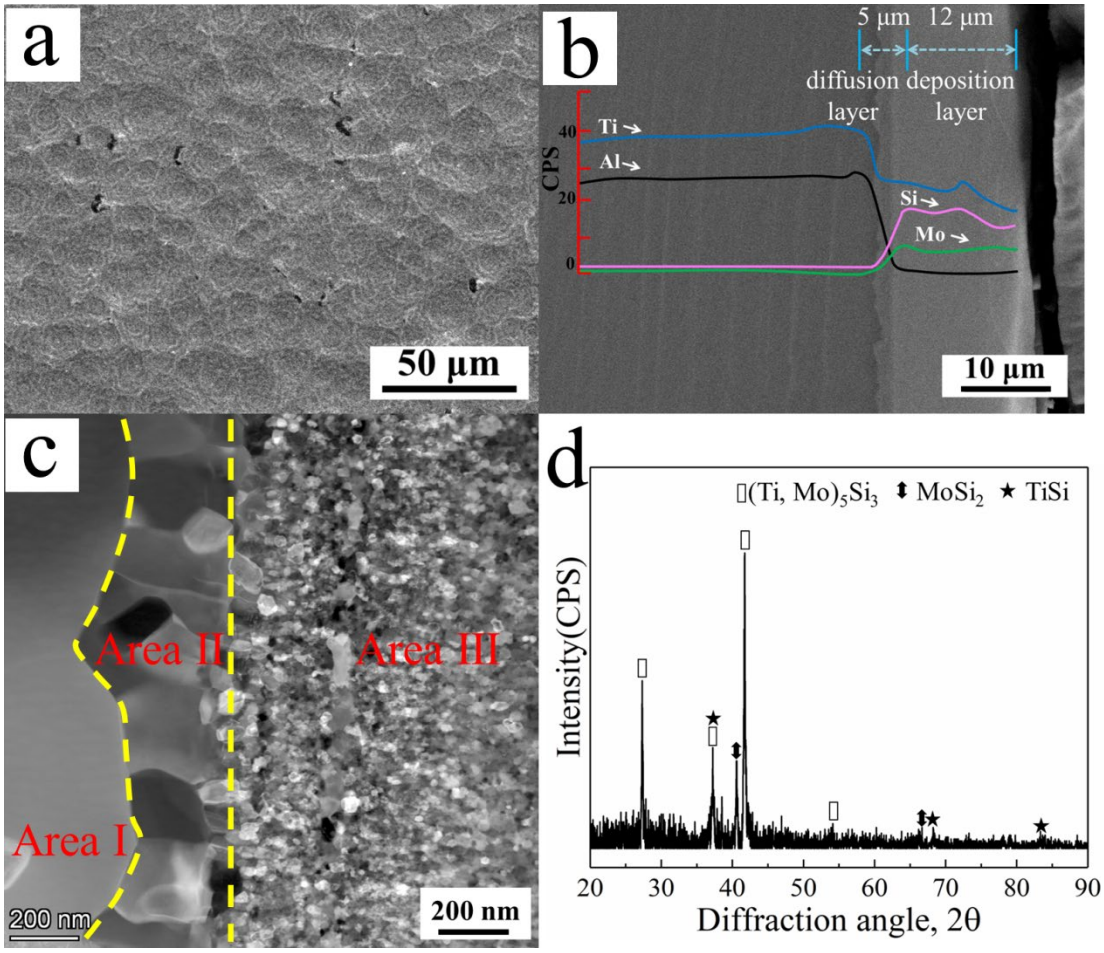

Fig. 1 The surface morphology (a), cross-sectional morphology with EDS scanning (b), TEM-DF image (c), and X-ray diffraction pattern (d), of coating.

Fig. 2 showed the AFM image of γ-TiAl and Mo-Si-Ti coating. Roughness (arithmetic average (Ra) and the root mean square (RMS)) and three-dimensional images of the samples were available from a flat topographic image of Fig. 2(a) and Fig. 2(c). The surface roughness of the substrate was 135 nm (RMS) or 106 nm (Ra). Scratches and bumps can still be observed on the surface of the polished substrate as shown in Fig. 2(b). The Mo-Si-Ti coating exhibits a similar roughness as the substrate, i.e., 141 nm (RMS) or 114 nm (Ra). The pits and bumps on the coating surface caused by the bombardment of argon ions can be clearly observed from Fig. 2(d).

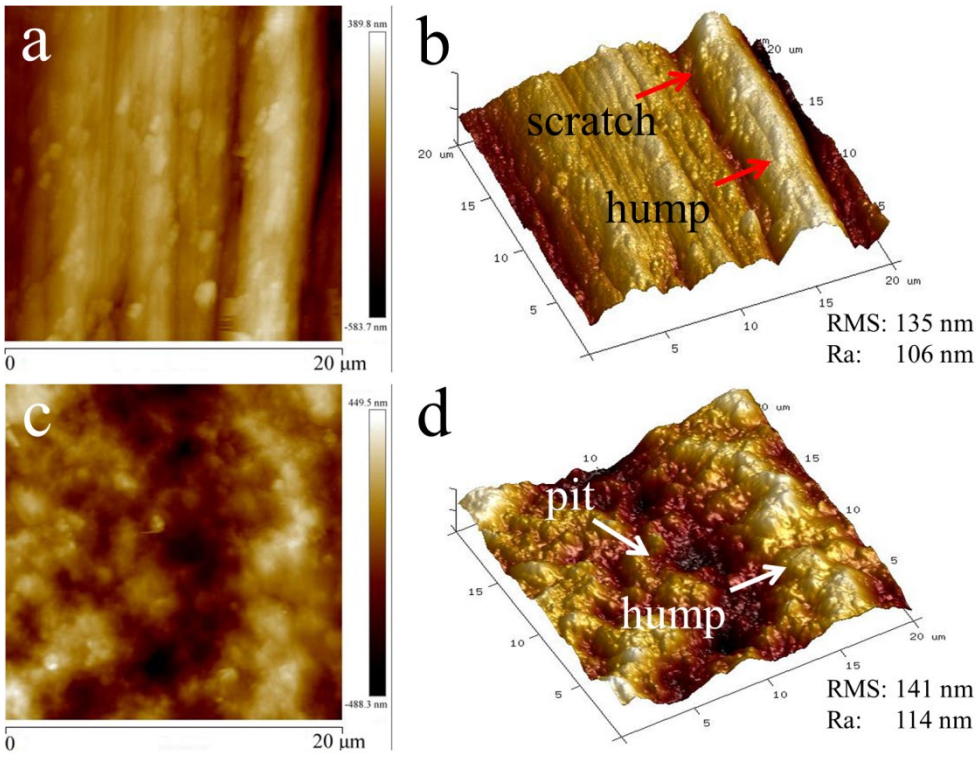

Fig. 2 AFM images of γ-TiAl (a, b) and Mo-Si-Ti coating (c, d)

3.2 Mechanical properties

Fig. 3 presented the nano-indentation results of γ-TiAl substrate and coating. The plastic work ($W_{plastic}$) of the sample could be determined by calculating the area between the loading and unloading curves, in Fig. 3a [27]. The substrate had a higher $W_{plastic}$ than the coating, indicating that the substrate experienced more plastic deformation during the test. The hardness (H), elasticity modulus (E), H/E and H^3/E^2 values of the substrate and the coating were approximately 8.4 and 19.6 GPa, 167.2 and 251.8 GPa, 0.050 and 0.078, and 0.021 and 0.119 GPa, respectively (Fig. 3b & 3c). The coating had a significantly higher hardness compared to the substrate. Furthermore, the coating exhibited a high resistant to plastic deformation and load bearing capacity, as indicated by the values of H/E and H^3/E^2 [28].

$$\varphi = \frac{E}{H}\left(\frac{\sigma}{\beta}\right)^{\frac{1}{2}} \quad (2)$$

where φ stands for the plasticity index, σ stands for the surface roughness, and β stands for the asperity radius.

$$N < 5.618\alpha^3 R^2 \frac{H^3}{E^2} \quad (3)$$

where R represents the radius of the contact sphere and α represented a constant.

According to equation 2, the plasticity index of the sample is related to the surface roughness (σ), asperity radius (β) and the H/E. From the AFM image, it could be observed that the substrate and coating had similar roughness as well as three-dimensional morphology, indicating that the parameters σ and β did not caused a significant difference of plasticity index between the substrate and the coating. However, the substrate and coating exhibited large differences of H/E value. The plasticity index was inversely proportional to H/E, indicating that Mo-Si-Ti coating with high H/E value had a high resistant to plastic deformation. Equation 3 provided a way to use sphere-on-flat Hertzian contact theory for calculating the maximum normal load (N) that could be applied without causing obvious plastic deformation. A sample with a high H^3/E^2 value could bear higher normal load [29, 30]. This also could be explained by the elastic-plastic deformation work. The zone between the loading and unloading lines stands for the plastic work ($W_{plastic}$) of the sample. Fig. 3d presented the $W_{elastic}$ and K values ($W_{elastic}/W_{plastic}$) of coating and substrate during nanoindentation test. Coating exhibited higher K values than substrate, indicating that the elastic work during the nanoindentation test was greater than the plastic work. Applying the same load to the surface, the coating with high K value would produce more elastic deformation to disperse the stress, allowing it to withstand a greater load before plastic deformation occurred.

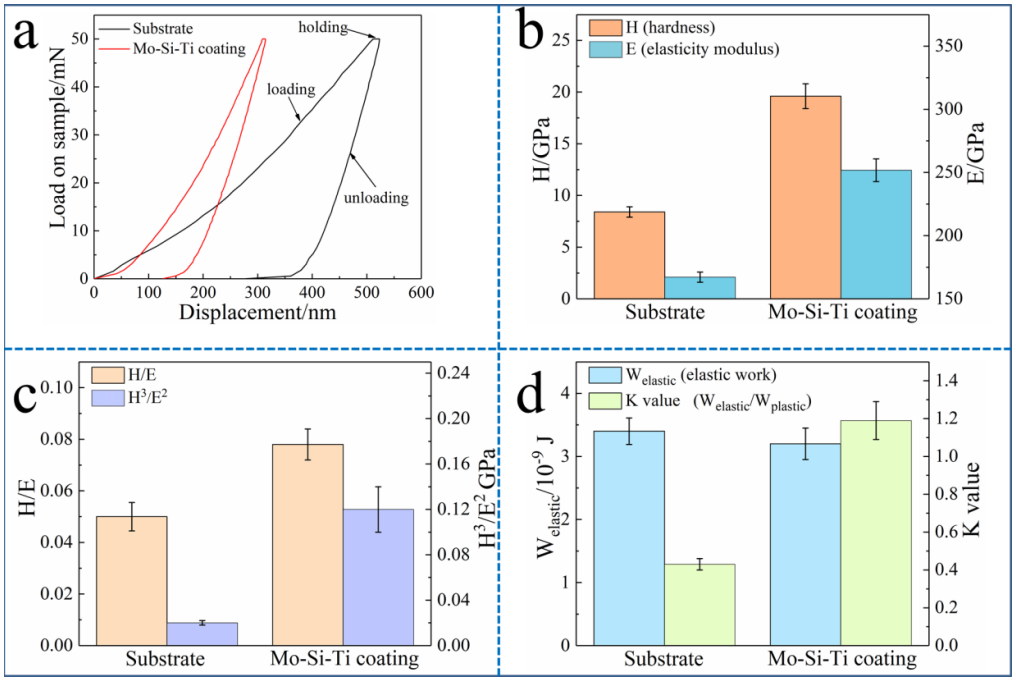

Fig. 3 Nano-indention results of γ-TiAl subatrate, Mo-Si-Ti coating (a) load versus displacement curves, (b) value of H and E, (c) H/E and H^3/E^2 parameters and (d) $W_{elastic}$ and K values.

Besides nanomechanical properties, fracture toughness is also a key factor affecting the wear resistance of the substrate and coating, which could be evaluated by the fracture type on the residual indent imprints, as shown in Fig. 4. Cracks parallel to the indentation edge and radial cracks (inside the indentation and diagonally) were found on the substrate surface, which indicated a low fracture toughness of substrate. No obvious cracks were observed on the surface of plasma based-Mo-Si-Ti coating and the coating exhibited high fracture toughness. The coating toughening mechanism could be explained in terms of crack generation and propagation based on the coating structure, stress field and residual stress. Firstly, according to the analysis of nanomechanical properties, more of the external loading force was dissipated as an elastic release, which could inhibit the generation and propagation of cracks [20]. Secondly, Mo-Si-Ti coating with gradient structure allowed a gradual transition of mechanical properties between the substrate and coating, which could reduce the generation of cracks due to the sudden changes of properties between the substrate and coating and enhance the fracture toughness. As shown in TEM-DF image, grain refinement occurred on the surface of substrate which contributed to an increase of hardness on the substrate surface and promoted a gradual increase of hardness between the substrate and the coating. Third, the mechanical property difference and microstructure mismatch between $(Ti,Mo)_5Si_3$ and $MoSi_2$ and TiSi could cause high strains to accumulate at the interface. As the crack extended to the crack tip, the crack started to extend along the interface where the fracture energy was lower. The crack deflection consumed some of the energy [25, 31, 32]. Moreover, when the cracks came into contact with the ductile substrate, tensile stress caused by local deformation of the ductile phase could consume energy [24]. After some of the external energy was released, the remaining energy will not be enough to promote the generation and propagation of cracks. In addition to the above factors, the lack of obvious cracks on the coating also related to the residual compressive stress, which was beneficial to inhibit the generation and propagation of cracks. The highest diffraction peak

(2θ=41.74°) in the Mo-Si-Ti coating XRD result were selected to calculate the residual stress using the $\sin^2\psi$ method [33]. And the azimuthal angles were selected as 0°, 15°, 30° and 45°. The measured residual stress of the coating was -1.26 ± 0.07 GPa, exhibiting an residual compressive stress. The constant bombardment of Ar^+ during the deposition process caused residual compressive stresses on the coating surface, which was referred to as the ion peening effect [34]. As another source, the thermal stress caused by the coating preparation process also caused the residual stress. Due to lower coefficients of thermal expansion (CTEs) of the coating compared to the substrate, compressive residual stress was generated inside the coating as the temperature of the sample cooled.

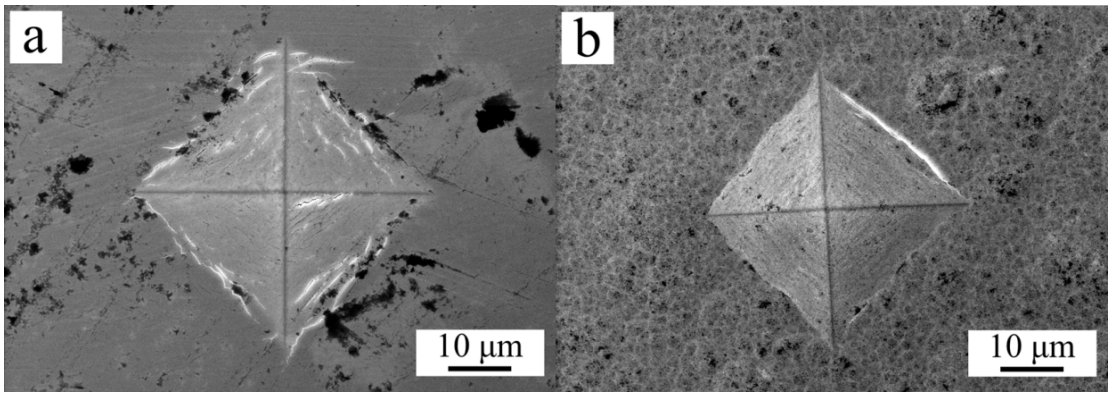

Fig. 4 Residual indent imprints on the γ-TiAl substrate (a) and the coating (b).

3.3 The effect of load on the tribological behaviors

Fig. 5, 6 and Table 1 depicted the morphology and composition of wear tracks at various loads. The substrate exhibited abrasive and oxidative wear. The presence of Si on the wear track indicated the transfer of material from load to substrate. As shown in the wear tracks of substrate, the friction between the substrate and the Si_3N_4 ball produced lots of wear debris. Meanwhile, during the reciprocal sliding process, some of debris was squeezed into the ends of the wear track (top A and B) and created grooves under external stress (in Fig. 5a1, b1 and c1). Moreover, some of the fine debris was pressed onto the surface of the wear track, forming a compacted layer. The oxide film was generated on the surface of the wear track, as O was found in the EDS results. And, as the load increased from 420 g to 820 g, the oxygen content on the surface of the wear track increased from 4.2 at.% to 10.0 at.%, refer O content for point 1 to 3 in Table 1,

indicating that the high load promoted the oxidation of substrate. The coating, in Fig. 6, also exhibited abrasive and oxidative wear. However, the oxidative wear of the coating was greater than that of the substrate because more O content (about 20 at.% - 30 at.%) was observed in the EDS results, refer O content for point 4 to 7 in Table 1. As shown in the TEM-DF image (Fig. 1), the coating exhibited smaller grain size than that of substrate. The more boundaries provided by the fine grains acted as "channels" to promote the inward diffusion of O, and allowed the effective oxygen diffusion coefficient of coating to be greater than that of substrate [35]. As a result, the coating was more easily oxidized and exhibited higher O content on the wear track surface.

$$\varepsilon \propto \frac{c}{d^2}\left(a + \frac{b}{d}\right) \quad (4)$$

where ε is creep rate; d is grain size; a b and c are not related to grain size [36].

Moreover, as shown in the equation 4, the presence of small grain size in the coating facilitated high creep rate, which could relieve stress in the oxide film and thus improve the adhesion between the coating and the oxide film [36]. Consequently, the wear tracks of the coating were smooth. However, when the load was increased to 820 g, some pits caused by the flaking of coating could be observed, which related to the oxidation of coating. The oxidation degree of Mo-Si-Ti coating surface in different regions was different according to different O content, and the area around the flaked coating exhibited higher O content (36.8 at.%, the area 7 in Fig. 6c2). The friction heat produced oxide film on the coating surface and might also reduce its fracture toughness, which eventually led to the flaking of coating. Similar to the substrate, high load promoted the oxidation of the coating because the O content on the coating surface increased as the load increased.

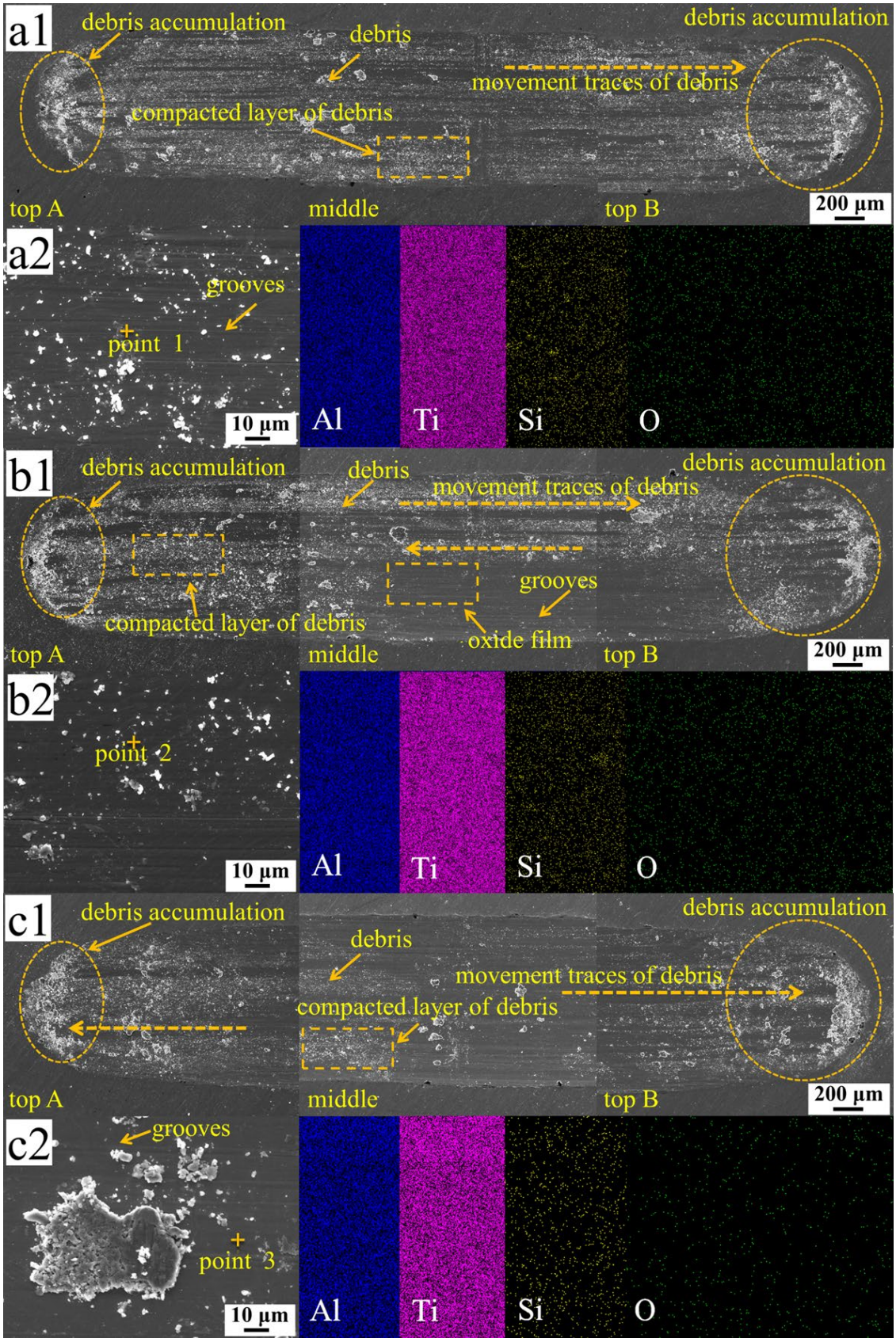

Fig. 5 SEM of the wear track of the substrate under various loads, enlarged morphology of the middle region of the wear track, mapping of the middle region of the wear track (a) 420 g, (b) 620 g and (c) 820 g.

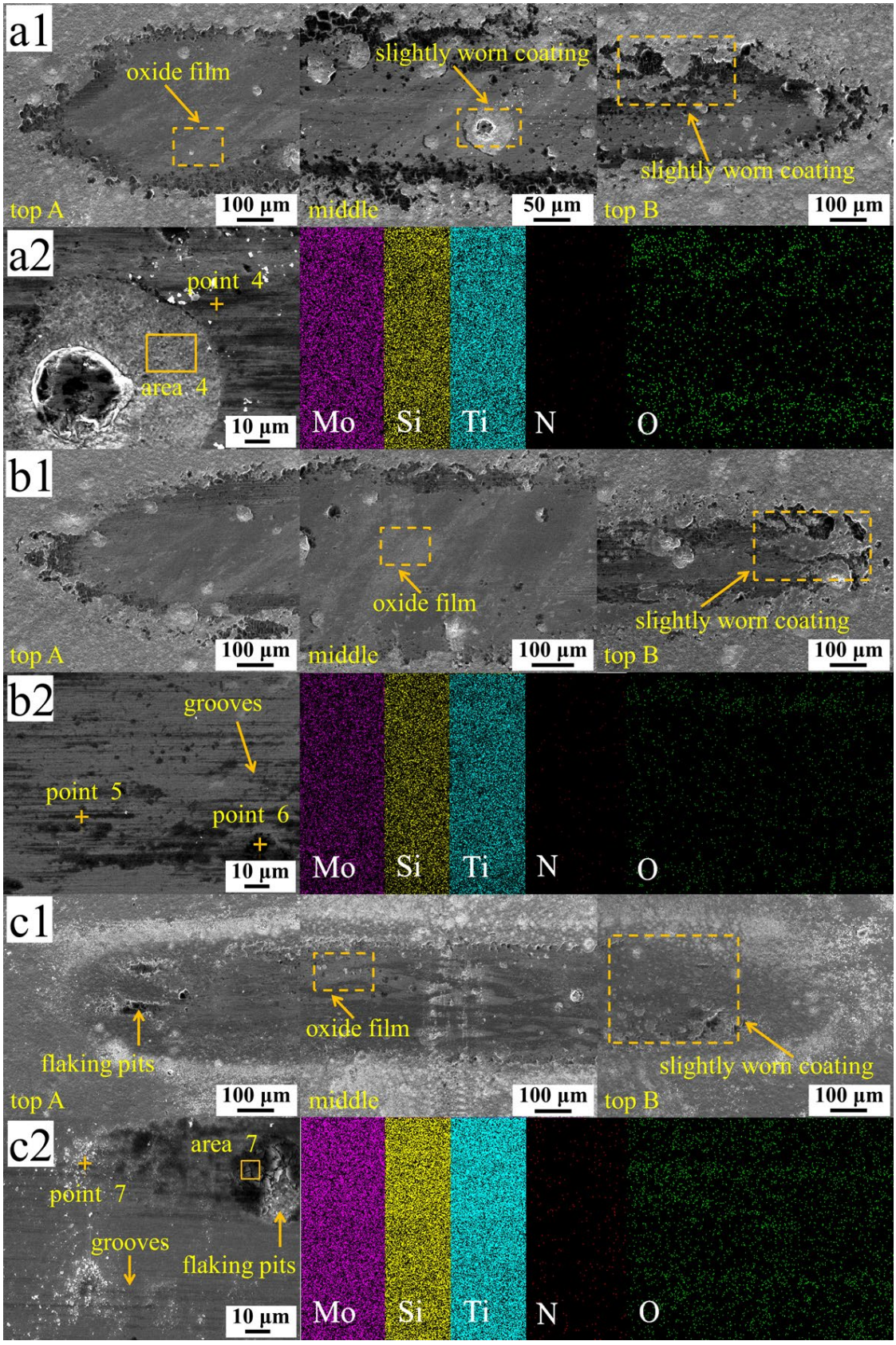

Fig. 6 SEM of the wear track of the coating under various loads, enlarged morphology of the middle region of the wear track, mapping of the middle region of the wear track (a) 420 g, (b) 620 g and (c) 820 g.

Table 1 EDS analysis of the wear tracks.

Analyzed point/area	Element content (at.%)					
	Al	Ti	Mo	Si	O	N
point 1	41.5	51.7		0.1	4.2	2.5
point 2	41.2	48.2		1.5	7.0	2.1
point 3	40.5	46.7		0.9	10.0	1.9
point 4		36.1	10.6	24.8	27.1	1.4
area 4		48.0	15.5	26.1	8.4	2.0
point 5		46.0	12.7	25.9	14.7	0.7
point 6		33.8	11.2	21.7	33.3	0
point 7		38.5	12.6	23.6	23.7	1.6
area 7		28.8	9.5	23.4	36.8	1.5

Fig. 7 presented the three-dimensional (3D) morphologies of wear tracks on the substrate and coating. The size of wear tracks on the coating surface including width and depth were significantly smaller than that of the substrate, indicating lower wear loss of the coating. As present in Fig. 8, the specific wear rates of the coating were 4.3, 4.0 and 3.5×10^{-6} $mm^3N^{-1}m^{-1}$ at loads of 420, 620 and 820 g, respectively. The specific wear rates of Mo-Si-Ti coating were reduced by 98.4, 98.1 and 97.9 % than that of the substrate. The coating exhibited better nanomechanical properties, such as high hardness, resistance to plastic deformation and load-carrying capacity, which could disperses external stress in the form of elastic deformation during the friction process and bear more load. High fracture toughness of coating reduced the generation of cracks and flaking of coating. As a result, the specific wear rate of coating was significantly lower than that of the substrate. Moreover, it was notable that the specific wear rate of both the substrate and the coating decreased with the increase of load, which was related to the wear debris and oxide film.

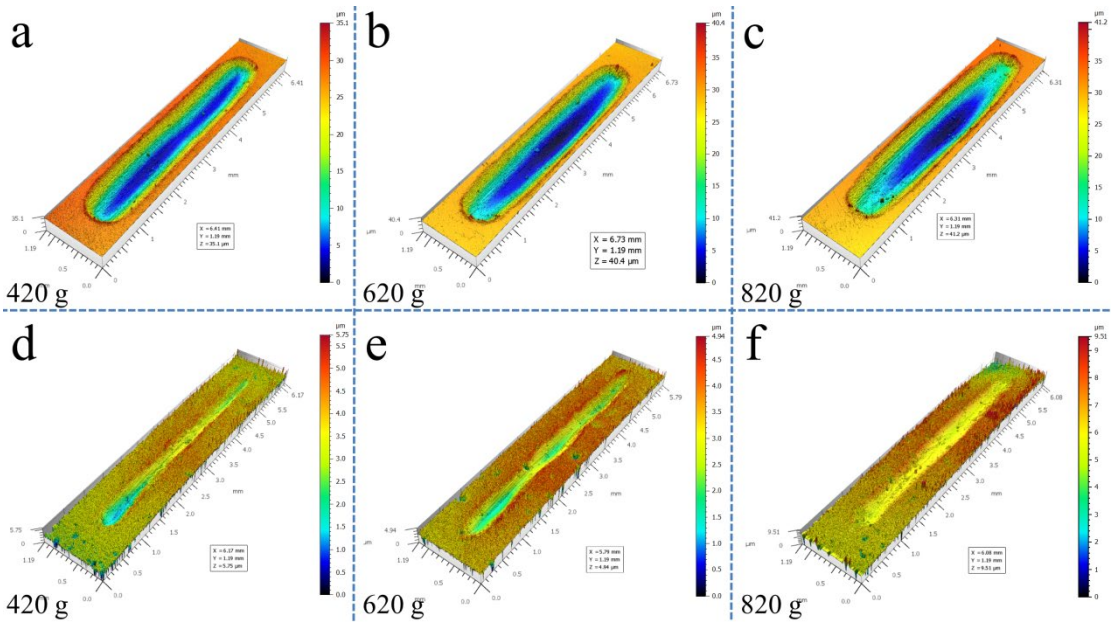

Fig. 7 Three-dimensional photography of wear surface at various loads (a) (b) and (c) substrate, (d) (e) and (f) coating.

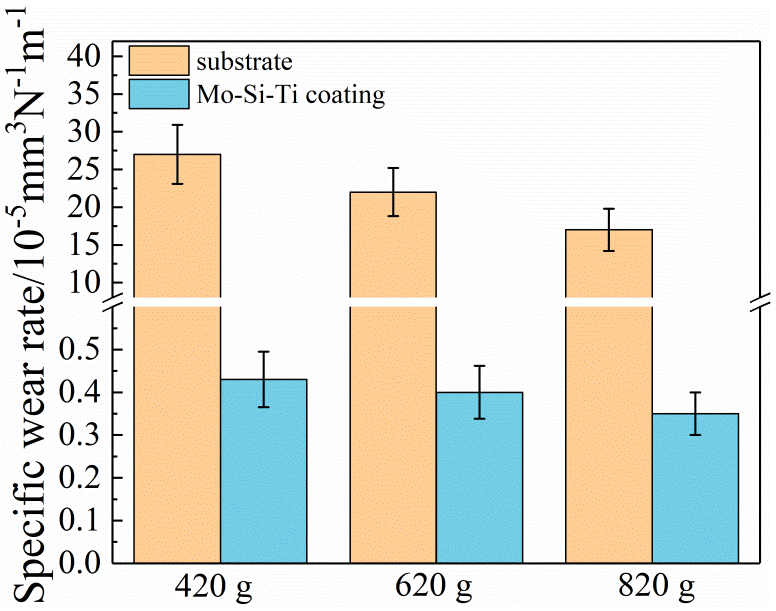

Fig. 8 Specific wear rates of substrate and coating at various loads.

3.4 Effect of debris and oxide layer on tribological behaviors

The wear morphology of the Si_3N_4 balls against the substrate and the Mo-Si-Ti coating at various loads were shown in SEM images in Fig. 9 and 10, respectively. The hardness of the Si_3N_4 ball (17.6 GPa, measured by nanoindentation test) was higher than that of the substrate (8.4 GPa), which resulted in less wear loss of the ball. Moreover, the reciprocating friction process caused the ball to exhibit an ellipse shape along the sliding direction. The wear loss of the ball increased as the load increased and

the wear track of the ball tended to be circular (Fig. 9a1, b1 and c1). Ti and Al from the substrate were visible on the Si_3N_4 ball wear track, as shown in the EDS of Fig. 9, indicating that the material transfer occurred between γ-TiAl substrate and Si_3N_4 ball. The existence of O proved the creation of an oxide film on the Si_3N_4 ball surface. Besides, some flaking pit (both in Fig. 9a2, b2, and c2) and obvious adhered wear debris (in Fig. 9c2) could be seen on the surface of the Si_3N_4 ball.

There were three main types of debris produced during the friction between the substrate and Si_3N_4 ball as shown in Fig. 9(a3, b3, and c3), namely plate shaped particles, large lump like wear debris and fine like wear debris. According to the results of the nanoindentation test, the substrate exhibited a low resistance to plastic deformation, which promoted adhesion between the substrate and the Si_3N_4 friction ball. Therefore, the adhered debris and flaking pits observed on the surface of the Si_3N_4 friction ball. Meanwhile, under the action of shear force during sliding process, the low fracture toughness of substrate promoted the crack nucleation and propagation on the surface of wear track, which caused the adhered substrate to flake off, as well as the generation of large lump like wear debris. An increase of plastic deformation under high load (820 g) resulted in an increase of large lump like wear debris. Moreover, the accumulation of plastic deformation led to the generation of plate shaped debris with an aspect ratio of 2-10. The formation of fine wear debris indicated that the oxide film on the wear track surface has been destroyed which was also could be observed in the EDS results of wear debris (Table 2) [37-39]. According to the EDS results in Table 2, it could be seen that the substrate, affected by less frictional heat generation, flaked off to form a large lump like wear debris, which made its O content (Point 1, 3 and 5) lower than that of fine wear debris. Meanwhile, it was inferred that the large lump like wear debris was composed of both the oxide and the substrate material. The fine wear debris formed by the fracture of oxide film contained more O and was mainly composed of oxides. Moreover, the O content of fine wear debris increased as the load increased, indicating that the high load promoted frictional heat generation as well as the formation and fracture of the oxide film, which agreed with the results of the O content on the surface of the wear track. The presence of Si and N in the wear debris indicated that the

Si_3N_4 ball was worn to form a small amount of wear debris.

The hardness of the Mo-Si-Ti coating (19.6 GPa) was higher than that of the Si_3N_4 ball (17.6 GPa), which led to a higher wear loss of the Si_3N_4 ball and made the Si_3N_4 ball to exhibit a circular shape and smoother wear track surface, refer Fig. 10. Moreover, the oxide film was generated on the Si_3N_4 ball surface as the presence of O was observed in the EDS. The high resistance to plastic deformation and fracture toughness of the coating reduced the generation of cracks and flaking during the friction process, resulting in less wear debris, and it was difficult to observe by SEM. Therefore, the wear debris generated during the friction between the coating and the Si_3N_4 ball was not characterized.

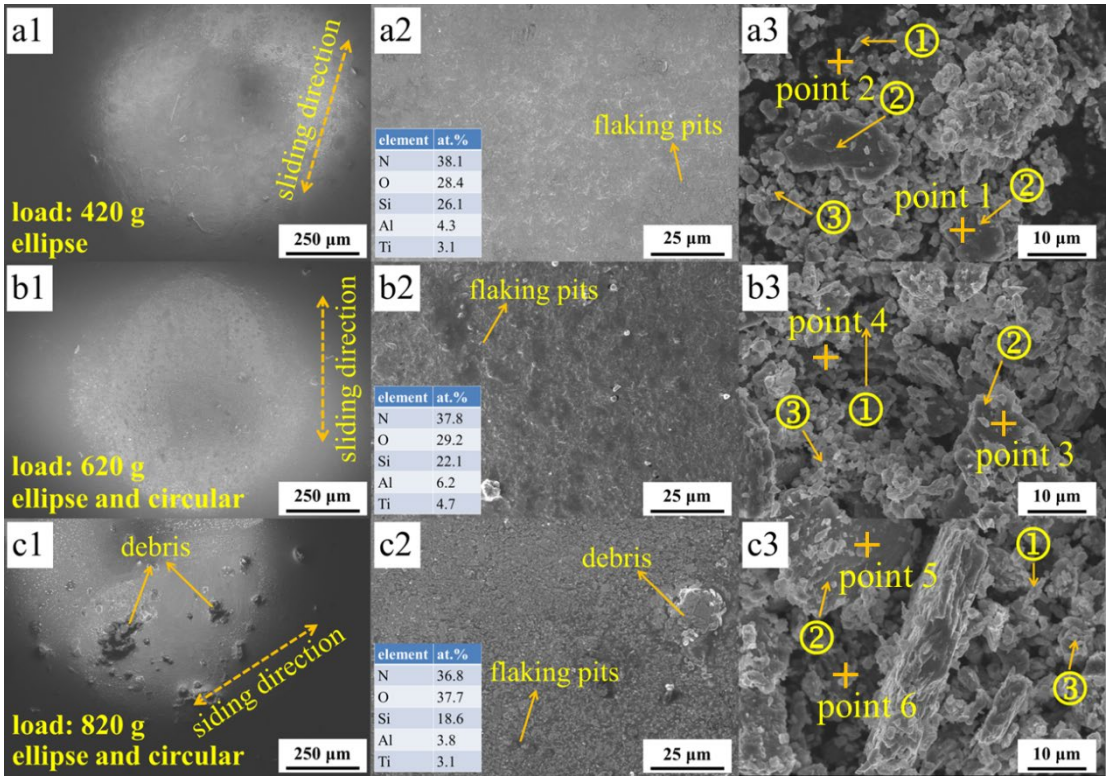

Fig. 9 The wear morphology on the Si_3N_4 balls against the substrate and debris. (a1), (a2), (b1), (b2), (c1) and (c2) are the wear morphology of Si_3N_4 balls. (a3), (b3) and (c3) are the morphology of debris. ①: Plate shaped particles; ②: Large lump like wear debris; ③: Fine or powder like wear debris.

Table 2 EDS analysis of the wear debris marked in Fig. 9.

Analyzed point	Element content (at.%)				
	Al	Ti	O	Si	N
point 1	23.41	33.85	28.79	0.19	13.76
point 2	15.16	23.86	37.72	0.28	22.98
point 3	29.24	31.36	22.26	1.15	15.99
point 4	20.00	25.15	34.80	0.53	19.52
point 5	27.12	33.65	20.80	1.31	17.13
point 6	14.52	20.44	41.83	0.79	22.42

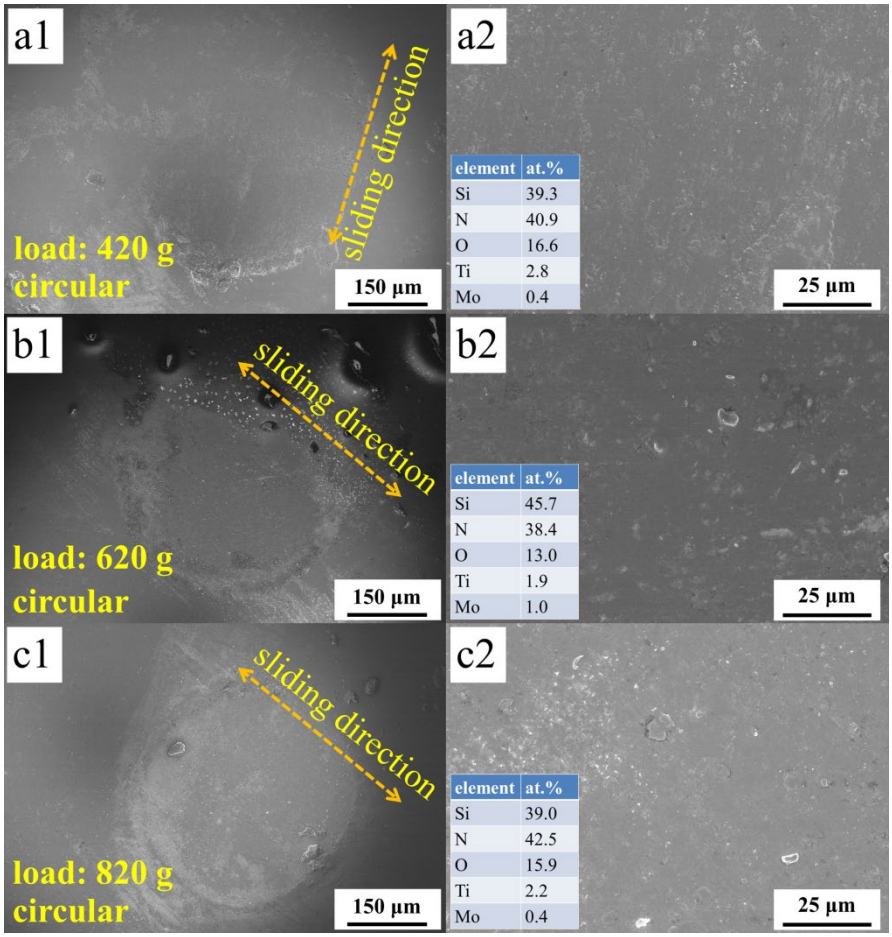

Fig. 10 The wear morphology on the Si_3N_4 balls against the coating (a1), (a2), (b1), (b2), (c1) and (c2) are the wear morphology of Si_3N_4 balls.

3.4.1 The effect of wear debris on the tribological behavior

Fig. 11 showed the friction coefficient curves of the substrate and coating during friction with Si_3N_4 ball. As shown in Fig. 11, both the substrate and the coating exhibited low friction coefficients at the initial stage of friction (before 2 min of wear test). The friction coefficients of the substrate and coating increased as the wear test

time increased, and then the friction process entered the stabilization stage. When the loads were 420 g and 620 g, the average friction coefficients of the substrate at the stabilization stage of friction were about 0.6. As the load increased to 820 g, the high load shortened the initial friction stage of substrate while slightly reducing the friction coefficient value (about 0.5) and also reduced the fluctuation amplitude of the friction coefficient at the stabilization stage. At loads of 420 g and 620 g, the coating exhibited a similar average friction coefficient to that of the substrate, which was about 0.6, but the friction coefficient of the coating had lower fluctuation amplitude. Moreover, different from the substrate, a slight increase of the friction coefficient for the coating was observed when the load was increased to 820 g. The substrate and coating produced various wear products during friction against the Si_3N_4 ball and affected the tribological behavior in different ways.

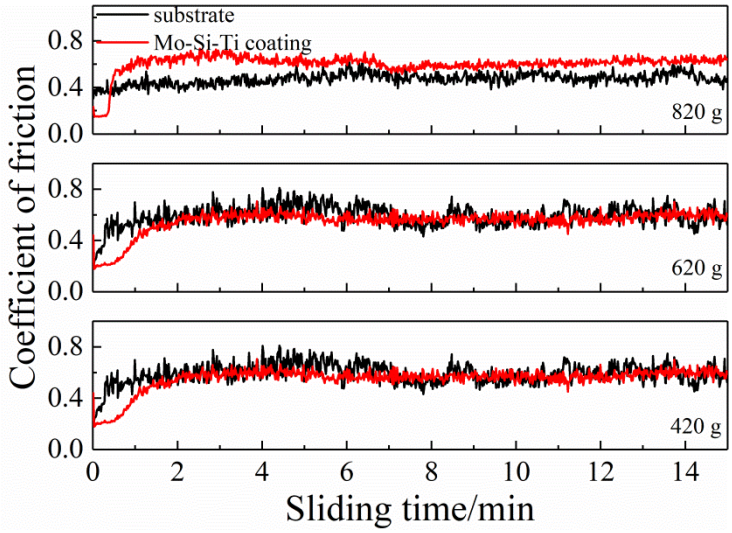

Fig. 11 Friction coefficient curves of substrate and coating under various loads

The debris had three effects on the tribological behavior of the γ-TiAl substrate and only affected the tribological behavior of Mo-Si-Ti coating at the initial stage of friction, as illustrated in the schematic diagram of Fig. 12a, b, c and d. (1) The debris served as a solid lubricant at the initial stage of friction. At the initial stage of friction, bumps on the surface of substrate and coating were contacted with Si_3N_4 ball and fracture under stress to form wear debris. The short initial stage of friction made the wear debris difficult to be oxidized significantly due to less friction heating generation. As a result, the wear debris formed at the initial stages of friction exhibited a similar

hardness to that of the substrate as well as the coating. Meanwhile, these wear debris act as a solid lubricant during the sliding process, thus reducing the friction coefficient and the wear rate. (2) The debris with high hardness, as the third body abrasive particle in three-body condition, promoted the abrasive wear and increased the wear loss of substrate. The substrate, Si_3N_4 friction ball, and the common oxides of the substrate after oxidation, i.e., TiO_2 and Al_2O_3, were given in Table 3.The hardness of TiO_2 (16.5 GPa) and Al_2O_3 (25-29 GPa) was significantly higher than that of the substrate (8.4 GPa). Moreover, debris adhered to the surface of the Si_3N_4 ball and then followed them in a reciprocating sliding. Under repeated external stress, the debris would flake off from the surface of the Si_3N_4 ball, removing some Si_3N_4 material with high hardness (17.6 GPa). The wear debris with high hardness could destroy the wear track surface and caused grooves. Variations in the morphology of wear track altered the conformity between surfaces and resulted in a redistribution of loads between asperities [40, 41]. Interactions between grooves, wear debris, asperities and reciprocating sliding caused crack initiation and extension, which resulted in the local removal of γ-TiAl from the wear track [42]. Therefore, the wear debris with high hardness increased the wear rate of substrate. Compared to the substrate, the coating produced only little wear debris at the initial stage of friction and the debris were removed from the wear track surface during the subsequent friction process. Therefore, the wear debris did not significantly affect the tribological behavior of the coating at the stabilization stage of friction.

Table 3 The hardness of different materials

	Hardness (GPa)	Source
γ-TiAl	8.4	Nanoindentation test
TiO_2	16.5	Reference [43]
Al_2O_3	25-29	Reference [44]
Si_3N_4	17.6	Nanoindentation test

(3) A protective transfer layer was formed by pressing some fine debris on the surface of the wear tracks. Oxidation, ploughing and compaction resulted in the creation of a protective transition layer on the surface of the substrate and the compacted layer of debris reduced the wear rate. As presented in Fig. 8, the specific wear rate of the

substrate gradually decreased as the load increased. Therefore, it could be inferred that the contribution of the compacted layer to reducing the wear rate was more significant than the contribution of debris to increasing wear rate through three body wear. However, the protective effect of the compacted layer appeared to be weakened in the present study. Because large debris created isolated obstructions on the surface of wear track and moved following the Si_3N_4 ball, which could destroy the completeness of the compacted layer.

3.4.2 The effect of oxide film on the tribological behavior

In addition to forming a compacted layer, wear debris could contribute to the friction heating. Adhered wear debris formed new micro-asperities during the friction process. The micro cutting heat generated by the ploughing effect between the micro-asperities and the wear tracks caused local high-temperature area. On the one hand, friction heating facilitated the plastic deformation and increased the wear rate. On the other hand, friction heating promoted the formation of oxide film, which could reduce the wear rate.

According to the wear tracks morphology (Fig. 4 and 5) and EDS (Table 1), an oxide film was generated on the surface of both the substrate, coating and the Si_3N_4 ball, allowing an oxide film-oxide film contact during wear tests. The increase of load had different effects on the tribological behavior of substrate and coating, both positive and negative. The debris could create grooves on the wear track surface under high load, destroying the continuity of the oxide film and thus weakening its protective effect. Then O reacted with the fresh γ-TiAl to form a new oxide film. Wear loss was increased by the repeated creation and removal of an oxide film [45]. Moreover, high load contributed to the friction heating generation and promoted the formation of oxide film as well as greater coverage. The presence of oxide film provided lower shearing energy junctions and reduced the frictional force, resulting in a low friction coefficient as well as the low wear rate [46]. Therefore, when the load was increased to 820 g, the O content on the wear track surface of substrate increased and was accompanied by a decrease of the friction coefficient. The specific wear rate of the substrate decreased as

load increased, indicating that the removal rate of oxide film did not exceed the formation rate of oxide film.

Friction heat generation had a higher effect on the coating than on the substrate, as more O content appeared on the wear track of coating. Meanwhile, the fine grain, high hardness and resistance to plastic deformation of the coating could support the oxide film and reduce the flaking of the oxide film. As a result, the fluctuation amplitude of the friction coefficient of the coating was smaller than that of the substrate attributed to the complete oxide film. However, when the load was increased to 820 g, high load caused the coating to flake off and the flaking pits appeared on the wear track of the coating surface, which caused a slight increase of the friction coefficient as well as an increase of the wear rate. Similar to the substrate, the specific wear rate of the coating decreased as the load increased, indicating that the contribution of the oxide film to reducing the wear rate was more significant than the contribution of oxide film to increasing wear rate through flaking off.

In addition to the debris and oxide film, the wear rate might also be affected by the strain hardening. γ-TiAl with a lower resistance to plastic deformation might be more easily strain hardened during friction process, resulting in smaller contact area and plastic regions, and thus reduced the specific wear rate [47, 48].

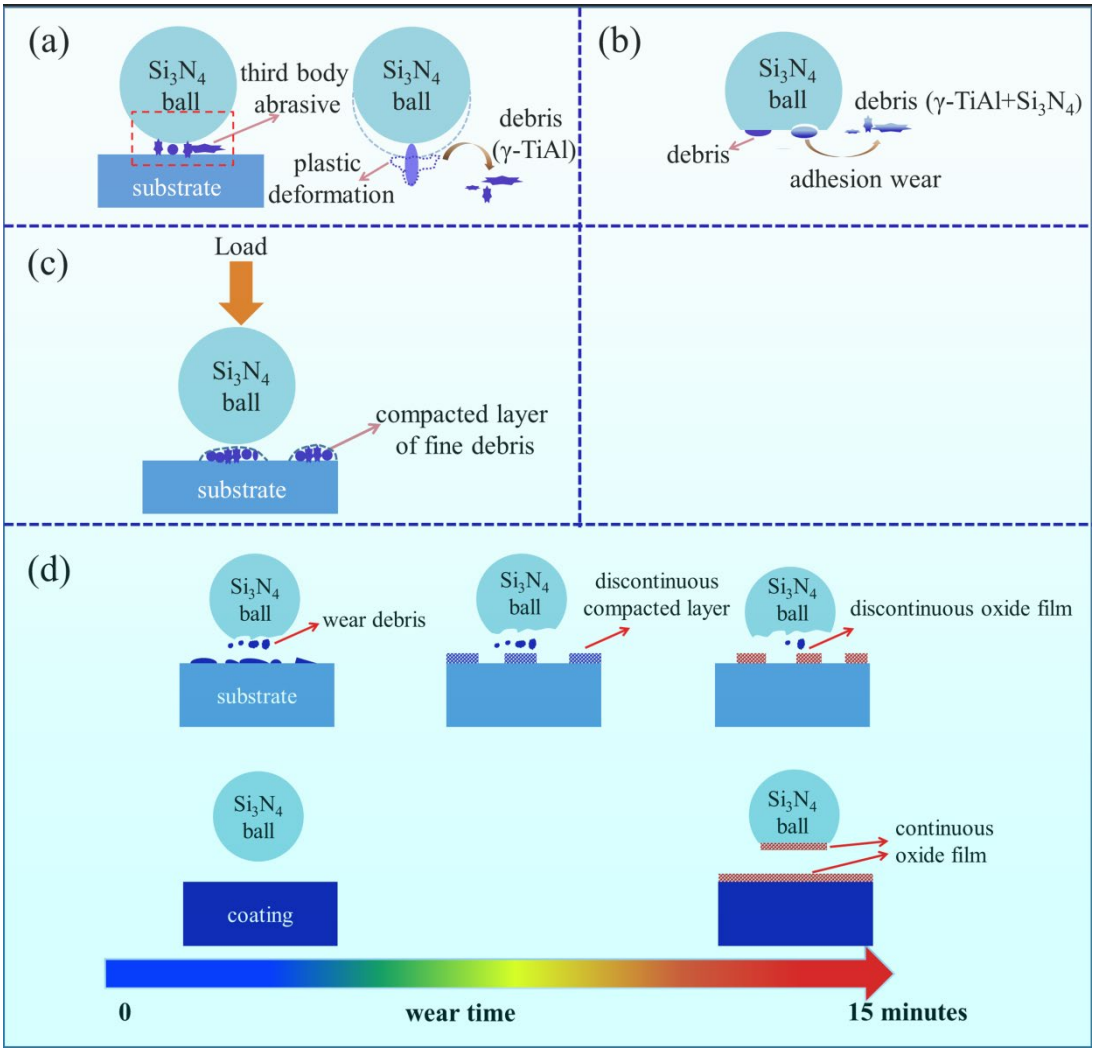

Fig. 12 Schematic diagram illustrated the wear mechanisms of the substrate and coating.

5. Conclusion

In present work, Mo-Si-Ti coating with a gradient structure was prepared on the γ-TiAl surface using a DGP technology to reduce the fracture and improve the wear resistance. The key conclusions were shown below:

(1) The Mo-Si-Ti coating consisting of the $(Ti, Mo)_5Si_3$, $MoSi_2$ and TiSi exhibited a composition and structure gradient. The interdiffusion of Al, Ti, Mo, and Si promoted the composition gradient of coating. The gradual decrease of grain size from the substrate to the coating allowed the coating to exhibit a structure gradient.

(2) The hardness and elasticity modulus of Mo-Si-Ti coating were 19.6 and 251.8 GPa, respectively, which were 2.3 and 1.5 times that of the γ-TiAl substrate. Higher

H/E and H^3/E^2 values indicated a better resistance to plastic deformation and load bearing capacity of Mo-Si-Ti gradient coating. The gradient structure inhibited the crack formation under external stress and allowed the coating to exhibit high fracture toughness, which ensured the excellent wear resistance.

(3) At various loads, the substrate and the coating showed abrasive and oxidative wear. The surface of the substrate suffered plastic deformation during friction, which led to lots of debris and higher wear rate. However, the formation of a compacted layer of debris and the oxide film caused the specific wear rate of the substrate to decrease as the load increased.

(4) The gradient structure with high nanomechanical properties as well as high fracture toughness reduced the fracture and flaking of the coating during wear test. Fine grains promoted the generation of oxide film and also improved the adhesion between oxide film and coating, resulting in the decrease of specific wear rates. The specific wear rates of the coating were 4.3, 4.0 and 3.5×10^{-6} $mm^3N^{-1}m^{-1}$ at loads of 420, 620 and 820 g, exhibiting reductions of 98.4%, 98.1%, and 97.9% compared to the wear rates of the substrate, indicating that the Mo-Si-Ti coating could effectively improve the wear resistance of γ-TiAl. The DGP technology provides a method for the preparation of coating with gradient structure. It is particularly suitable for the coatings which have obvious different properties compared to the substrate, such as ceramic coating.

Acknowledgments

This project was supported by Natural Science Foundation for Excellent Young Scientists of Jiangsu Province, China (Grant No. BK20180068), China Postdoctoral Science Foundation funded project (Grant No. 2018M630555), Opening Project of Materials Preparation and Protection for Harsh Environment Key Laboratory of Ministry of Industry and Information Technology (Grant No. XCA20013-1) and China Scholarship Council.

References

[1] Bewlay BP, Nag S, Suzuki A, Weimer MJ. TiAl alloys in commercial aircraft engines. Materials at High Temperatures 2016; 33: 549-559.

[2] Bauer PP, Radosław S, Klamann L, Laska N. Aluminum diffusion inhibiting

properties of Ti_5Si_3 at 900 °C and its beneficial properties on Al-rich oxidation protective coatings on γ-TiAl. Corrosion Science 2022; 201: 110265.

[3] Clemens H, Smarsly W. Light-weight Intermetallic Titanium Aluminides-Status of Research and Development. Advanced Materials Research 2011; 278: 551-556.

[4] Fergus JW. Review of the effect of alloy composition on the growth rates of scales formed during oxidation of gamma titanium aluminide alloys. Materials Science and Engineering A 2002; 338: 108–125.

[5] Knaislová A, Novák P, Cabibbo M, Jaworska L, Vojtech D. Development of TiAl-Si Alloys-A Review. Materials 2021; 14: 1030.

[6] Wen DS, Kong BB, Wang SR, Zhang MY, Wang GQ, Wang XY, et al. Atomic-scale investigation on fretting wear mechanism of γ phase in a cast Ti-45Al alloy. Applied Surface Science 2021; 565: 150555.

[7] Mengis L, Grimme C, Galetz MC. High-temperature sliding wear behavior of an intermetallic γ-based TiAl alloy. Wear 2019; 427: 341-347.

[8] Yang YL, Wang CL, Gesang YZ, Shang HF, Wang R, Liang YM, et al. Fretting wear evolution of γ -TiAl alloy. Tribology International 2021; 154: 106721.

[9] Obert S, Kauffmann A, Heilmaier M. Characterisation of the oxidation and creep behaviour of novel Mo-Si-Ti alloys. Acta Materialia 2020; 184: 132-142.

[10] Obert S, Kauffmann A, Seils S, Schellert S, Weber M, Gorr B, et al. On the chemical and microstructural requirements for the pesting-resistance of Mo-Si -Ti alloys, Journal of Materials Research and Technology. 2020; 9: 8556-8567.

[11] Obert S, Kauffmann A, Seils S, Boll T, Kauffmann WS, Chen H, et al. Microstructural and chemical constitution of the oxide scale formed on a pesting-resistant Mo-Si-Ti alloy. Corrosion Science 2021; 178: 109081.

[12] Parthasarathy TA, Mendiratta MG, Dimiduk DM. Oxidation mechanisms in Mo-reinforced $Mo_5SiB_2(T_2)$-Mo_3Si alloys. Acta Materialia 2002; 50: 1857-1868.

[13] Zhao M, Xu BY, Shao YM, Zhu Y, Wu J, Wu SS, et al. Microstructure and

oxidation mechanism of multiphase Mo-Ti-Si-B alloys at 800 ℃. Corrosion Science 2021; 187: 109518.

[14] Schliephake D, Kauffmann A, Cong XN, Gombola C, Azim M, Gorr B, et al. Constitution, oxidation and creep of eutectic and eutectoid Mo-Si-Ti alloys. Intermetallics 2019; 104: 133-142.

[15] Anton R, Hüning S, Laska N, Weber M, Schellert S, Gorr B, et al. Interface reactions of magnetron sputtered Si-based dual layer coating systems as oxidation protection for Mo-Si-Ti alloys. Surface & Coatings Technology 2022; 444: 128620.

[16] Majumdar S, Paul B, Singh PK, Kishor J, Kain V. Effect of Si content on microstructure, mechanical and oxidation properties of hot pressed Mo-Ti-Si alloys. Intermetallics 2018; 100: 126-135.

[17] Narayana PL, Kim JH, Yun DW, Kim SE, Reddy NS, Yeom JT, et al. High temperature isothermal oxidation behavior of electron beam melted multi-phase γ-TiAl alloy. Intermetallics 2022; 141: 107424.

[18] Maliutina IN, Mohand HS, Sijobert J, Bertrand P, Lazurenko DV, Bataev IA. Structure and oxidation behavior of γ-TiAl coating produced by laser cladding on titanium alloy. Surface & Coatings Technology 2017; 319: 136-144.

[19] Lin NM, Zhang LX, Zou JJ, Liu Q, Yuan S, Zhao LL, et al. A combined surface treatment of surface texturing-double glow plasma surface titanizing on AISI 316 stainless steel to combat surface damage : Comparative appraisals of corrosion resistance and wear resistance. Applied Surface Science 2019; 493: 747-765

[20] Qi Y, Liang WP, Miao Q, Yi JW, Lin H, Liu YY. Role of the nitrogen ratio on mechanical properties and wear resistance of CrN/Fe functionally graded coating produced by double glow plasma alloying. Applied Surface Science 2022; 585: 152735.

[21] Lin NM, Liu Q, Xie RZ, Zou JJ, Li DL, Yuan S, Wang ZX, Ma Y, Liu XP, Wang ZH, Tang B. Research Progress in Strengthening Surface Performance of Iron and Steel Materials by Double Glow Plasma Surface Alloying

Technology: a Brief Review. Reviews on Advanced Materials Science 2017; 51: 16-34.

[22] Yuan S, Lin NM, Zeng QF, Zhang HX, Liu XP, Wang ZH, Wu YC. Recent developments in research of double glow plasma surface alloying technology : a brief review, Journal of Materials Research and Technology 2020; 9: 6859-6882.

[23] Quammen RN, Rottmann PF. Investigation of low temperature oxidation behavior of MoNbTaW thin films. Journal of Alloys and Compounds 2022; 900: 163373.

[24] Li QL, Song P, Lü KY, Dong Q, Li Q, Tan J, et al. Fracture behaviour of ceramic-metallic glass gradient transition coating. Ceramics International 2019; 45: 5566-5576.

[25] Bai HQ, Zhong LS, Shang Z, Xu YH, Wu H, Bai JM, et al. Microstructure and mechanical properties of TiC-Fe surface gradient coating on a pure titanium substrate prepared in situ. Journal of Alloys and Compounds 2019; 771: 406-417.

[26] E.P. EerNisse, S.T. Picraux, Role of integrated lateral stress in surface deformation of He-implanted surfaces, J. Appl. Phys. 48 (1977) 9–17.

[27] Oliver WC, Pharr GM. Measurement of hardness and elastic modulus by instrumented indentation : Advances in understanding and refinements to methodology. Journal of Materials Research 2004; 19: 3-20.

[28] Mandrino D, Podgornik B. XPS investigations of tribofilms formed on CrN coatings. Applied Surface Science 2017; 396: 554-559.

[29] Yi JW, Miao Q, Liang WP, Ding Z, Qi Y, Lin H, et al. A study for pre-processing of Nb diffusion in Nb-N layer by double-glow plasma alloying. Journal of Alloys and Compounds 2020; 820: 153121.

[30] Ehtemam-haghighi S, Cao GH, Zhang LC. Nanoindentation study of mechanical properties of Ti based alloys with Fe and Ta additions. Journal of Alloys and Compounds 2017; 692: 892-897.

[31] Wang YX, Zhang S. Toward hard yet tough ceramic coatings. Surface &

Coatings Technology 2014; 258: 1-16.

[32] He JY, Lan XX, Wan J, Liu HL, Liu ZW, Jiao DL. Modifying Cr/CrN composite structure by Fe addition: Toward manufacturing cost-effective and tough hard coatings. Applied Surface Science 2021; 545: 149025.

[33] O.P. Oladijo, L.L. Collieus, B.A. Obadele, E.T. Akinlabi. Correlation between residual stresses and the tribological behaviour of Inconel 625 coatings. Surface and Coatings Technology 2021; 419: 127288.

[34] C.A. Davis. A simple model for the formation of compressive stress in thin films by ion bombardment. Thin Solid Films 1993; 226: 30–34.

[35] L.H. Zhu, M.M. Hu, W.Y. Ni, Y.X. Liu. High temperature oxidation behavior of Ti0.5Al0.5N coating and Ti0.5Al0.4Si0.1N coating. Vacuum 2012; 86: 1795-1799.

[36] P. Pérez, J.A. Jiménez, G. Frommeyer, P. Adeva. The influence of the alloy microstructure on the oxidation behavior of Ti–46Al–1Cr–0.2Si Alloy. Oxidation of Metals 2000; 53: 99-124.

[37] Stachowiak GW, Podsiadlo P. Surface characterization of wear particles. Wear 1999; 229: 1171-1185.

[38] Stachowiak GW, Podsiadlo P. Characterization and classification of wear particles and surfaces. Wear 2001; 249: 194-200.

[39] Chen KM, Zhou Y, Li XX, Zhang QY. Wang L, Wang SQ. Investigation on wear characteristics of a titanium alloy/steel tribo-pair. Materials and Design 2015; 65: 65–73.

[40] Chen KM, Zhou Y, Li XX, Zhang QY. Wang L, Wang SQ. Investigation on wear characteristics of a titanium alloy/steel tribo-pair. Materials and Design 2015; 65: 65–73.

[41] Lim SC. Recent developments in wear-mechanism maps. Tribiology International 1998; 31: 87-97.

[42] El-thalji I, Jantunen E. Dynamic modelling of wear evolution in rolling bearings. Tribiology International 2015; 84: 90-99.

[43] E. Rayón, V. Bonache, M.D. Salvador, E. Bannier, E. Sánchez, A. Denoirjean,

H. Ageorges. Nanoindentation study of the mechanical and damage behaviour of suspension plasma sprayed TiO2 coatings. Surface and Coatings Technology 206 (2012) pp. 2655-2660.

[44] S. Ruppi, A. Larsson, A. Flink. Nanoindentation hardness, texture and microstructure of α-Al_2O_3 and κ-Al_2O_3 coatings. Thin Solid Films 2008; 516: 5959-5966.

[45] Yang LQ, Xue WH, Gao SY, Liu HW, Cao YF, Duan DL, et al. Study on sliding friction and wear behavior of M50 bearing steel with rare earth addition. Tribology International 2022; 174: 107725.

[46] Tyagi R, Xiong DS, Li JI. Effect of load and sliding speed on friction and wear behavior of silver/h-BN containing Ni-base P/M composites. Wear 2011; 270: 423-430.

[47] Zhao JH, Nagao S, Zhang ZL. Loading and unloading of a spherical contact : From elastic to elastic-perfectly plastic materials. International Journal of Mechanical Sciences 2012; 56: 70-76.

[48] Wang F, Keer LM. Numerical Simulation for Three Dimensional Elastic-Plastic Contact With Hardening Behavior. Journal of Tribology 2005; 127: 494-502.